AMERICAN ACADEMY OF OPHTHALMOLOGY®

Quantitative Multimodal Imaging Characterization of Intraretinal Cysts versus Degenerative Pseudocysts in Neovascular Age-Related Macular Degeneration

Alessandro Arrigo, MD, PhD,[1,2] *Emanuela Aragona, MD, PhD,*[1] *Maurizio Battaglia Parodi, MD,*[1] *Francesco Bandello, MD*[1]

Objective: To differentiate intraretinal fluid (IRF) cysts from degenerative pseudocysts in neovascular age-related macular degeneration (AMD) by quantitative multimodal imaging.

Design: Observational, cross-sectional.

Participants: Patients affected by macular neovascularization secondary to AMD.

Methods: All patients were analyzed by OCT, OCT angiography (OCTA), and dense automatic real-time (ART) OCTA. New-onset cysts were considered IRF, whereas those cysts that were found to be persistent for at least 3 months were categorized as degenerative pseudocysts. Intraretinal cysts were automatically segmented to calculate cyst circularity. Peri-cyst space was quantitatively analyzed to assess the presence of perfusion signal and hyperreflective foci (HF).

Main Outcome Measures: Best-corrected visual acuity, cyst circularity, peri-cyst perfusion, peri-cyst HF, fibrosis, and outer retinal atrophy.

Results: We analyzed 387 cysts collected from 35 eyes of 35 patients with neovascular AMD (14 men; mean age, 80 ± 5 years). We classified 302 IRF cysts and 85 degenerative pseudocysts. Intraretinal fluid cysts were characterized by significantly higher circularity (0.86; range, 0.81−0.91), perfusion signal in the peri-cyst space, and peri-cyst HF in 89% of cases (all $P < 0.05$). Degenerative pseudocysts showed significantly lower circularity (0.68; range, 0.64−0.76), no perfusion signal in the peri-cyst space, and peri-cyst HF in only 29% of cases (all $P < 0.05$). The adopted quantitative metrics significantly correlated with disease duration, number of injections, fibrosis, and outer retinal atrophy.

Conclusions: Intraretinal fluid cysts can be discriminated from degenerative pseudocysts using a quantitative multimodal imaging approach. These findings are clinically relevant and should be included in future training models for artificial intelligence algorithms to improve the diagnostic power and fluid monitoring in neovascular AMD.

Financial Disclosure(s): The author(s) have no proprietary or commercial interest in any materials discussed in this article. *Ophthalmology Retina 2024;8:1118-1126*

See Editorial on page 1115

Neovascular age-related macular degeneration (AMD) is a common complication characterized by fluid accumulation in the subretinal or intraretinal spaces and visual function deterioration.[1−3] Several studies have highlighted the significantly worse impact of intraretinal fluid (IRF) on disease progression, compared with subretinal fluid.[4−7] The pathogenesis of IRF can be both exudative and transudative. The exudative pathway recognizes a direct neovascular origin of the fluid.[8] The transudative pathway may be associated with different mechanisms, including the impairment of the inner blood−retinal barrier and Müller cell dysfunction.[8,9] A third type of IRF cysts detectable on OCT scans of neovascular AMD are degenerative pseudocysts. These cystoid cavities are characterized by the following: (1) localization in the inner retina; (2) lack of a direct neovascular origin; (3) persistence despite anti-VEGF treatments; and (4) association with later stages of neovascular AMD with their characteristic fibro-atrophic complications. The first OCT description of "retinal pseudocysts" was made in 2010 in geographic atrophy without macular neovascularization (MNV).[10] Later, these cysts were also described in neovascular AMD and were called "degenerative pseudocysts" or "cystoid macular degeneration."[11] In both cases, the term "pseudo" refers to the nonexudative origin of these cystoid spaces. Their presence in neovascular AMD has recently been confirmed by Monje-Fernández et al.[12]

The characterization of these different types of intraretinal cysts is extremely important to establish the proper treatment strategies. In addition, ever growing efforts are

https://doi.org/10.1016/j.oret.2024.05.019
ISSN 2468-6530/24

focused on developing artificial intelligence (AI)-based approaches to detect and monitor fluid changes in neovascular AMD.[13–15] In this context, a major unmet need is the categorization of different types of intraretinal cysts as pertaining to active disease or atrophic changes to appropriately analyze data sets and provide outputs that are helpful for developing treatment strategies. Indeed, the discrimination of "active" IRF cysts and "inactive" degenerative pseudocysts is fundamental to properly manage patients with neovascular AMD, considering both human graders and AI-based algorithms.

The purpose of the present study was to provide quantitative evidence based on multimodal imaging to discriminate intraretinal cysts from degenerative pseudocysts in neovascular AMD.

Methods

This study was designed as an observational, cross-sectional case series. Patients affected by neovascular AMD already receiving anti-VEGF treatments were recruited at the Ophthalmology Unit of IRCCS San Raffaele Scientific Institute, Milan. A signed informed consent was obtained from all patients before inclusion in the study. The entire study was conducted in accordance with the Declaration of Helsinki, and it was approved by the Ethical Committee of the IRCCS San Raffaele Scientific Institute, Milan (referral code MIRD2020). Patients received treatment with pro-re-nata or treat-and-extend regimens according to their ophthalmologists' discretion.

Inclusion/Exclusion Criteria and IRF Classification

The inclusion criteria were type 1, type 2, or mixed type MNV secondary to AMD. The following exclusion criteria were considered: newly diagnosed MNV lesions, type 3 MNV, and aneurysmal type 1 MNV. We also excluded patients with high-media opacity, any other type of retinal or optic nerve diseases, ophthalmic surgery within the last 3 months, and any uncontrolled systemic condition potentially affecting the results of the analyses. Only 1 eye for each patient was considered in the analyses. Intraretinal fluid and degenerative pseudocysts were classified according to the following criteria. Intraretinal fluid was defined as the transient appearance of intraretinal cysts at the study visit, i.e., without signs of the same cysts at the last follow-up (up to 3 months). Degenerative pseudocysts were defined as intraretinal cysts persisting for at least 3 months, despite the administration of intravitreal injections during this period of time, and colocalizing with clear signs of advanced fibrosis or outer retinal atrophy, as shown by OCT scans. This is the reason why we excluded newly diagnosed lesions, because of the possible lack of previous follow-up visits. Moreover, we excluded eyes with type 3 MNV or aneurysmal type 1 MNV to avoid the characteristically poor image quality and potentially severe disruption of macular anatomy.

Data Collection

Ophthalmic examination included best-corrected visual acuity (BCVA) measurement using standard ETDRS charts, slit-lamp examination of anterior and posterior segments, and Goldmann applanation tonometry. Structural OCT and OCT angiography (OCTA) images were acquired by means of a Spectralis HRA2+OCT device (Heidelberg Engineering GmbH). The structural OCT acquisition protocol included raster, radial, and dense scans with automatic real-time (ART) >25 and enhanced depth imaging. OCT angiography acquisitions included high-resolution scans (125 kHz; ART 7; volume 15° × 15°; interslice gap 11 μm), and dense ART (DART) OCTA (125 kHz; ART 100; volume 10° × 0.5° retinal eccentricity; isotropic sampling density 6 μm). We included only acquisitions with HEYEX quality score of >25.

Intraretinal Cyst OCT Analyses

We included only cysts with a diameter of >50 μm to avoid possible image resolution biases. Each cyst was classified in accordance with the above-described criteria and was analyzed separately, on both structural OCT and enface OCT scans where the same cyst was segmented in a consistent manner in both images. In brief, from structural OCT, we segmented each cyst b-scan by b-scan. From enface OCT, we segmented each cyst considering its entire segmentation. In both cases, the segmentation was done using a semiautomatic approach based on the ImageJ package[16] to avoid biases related to manual segmentation of the cysts. The images were exported in TIFF format and loaded in ImageJ.

For structural OCT images, we used the following pipeline for all the slabs showing each cyst: cyst isolation (selection of the cyst and the retinal structures around the cyst) → cyst segmentation (using the thresholding function *set to black* [0–20 pixel intensity]) → cyst boundary selection (using the ImageJ *Skeletonize* function) → calculation of cyst circularity (ImageJ formula: $4 \cdot \pi$[area]/[perimeter^2]). The final circularity value corresponded to the mean of the circularity calculated on each OCT slab. This pipeline is depicted in Figure 1.

For enface OCT images, we used the following pipeline for the entire cyst segmentation image: cyst isolation (selection of the cyst and the retinal structures around the cyst) → cyst segmentation (using the thresholding function *set to black* [0–20 intensity pixels]) → cyst boundaries selection (using the ImageJ *Skeletonize* function) → calculation of cyst circularity (ImageJ formula: 4π[area]/[perimeter^2]). In this case, we collected one circularity value for each included cyst. The pipeline is shown in Figure 2. We also

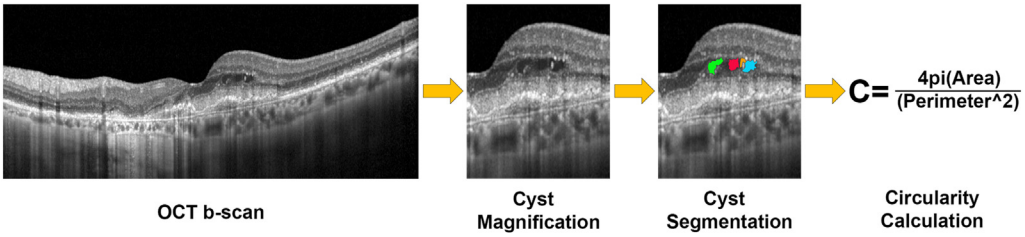

Figure 1. Schematic representation of cyst segmentation and circularity calculation based on OCT b-scan. For each OCT b-scan showing intraretinal cysts, we performed the automatic segmentation, by only selecting the black pixels (i.e., intensity range, 0–20) (manually colored in this figure). Each cyst is separately considered for circularity calculation. The final circularity value corresponds to the mean value obtained from all OCT b-scans.

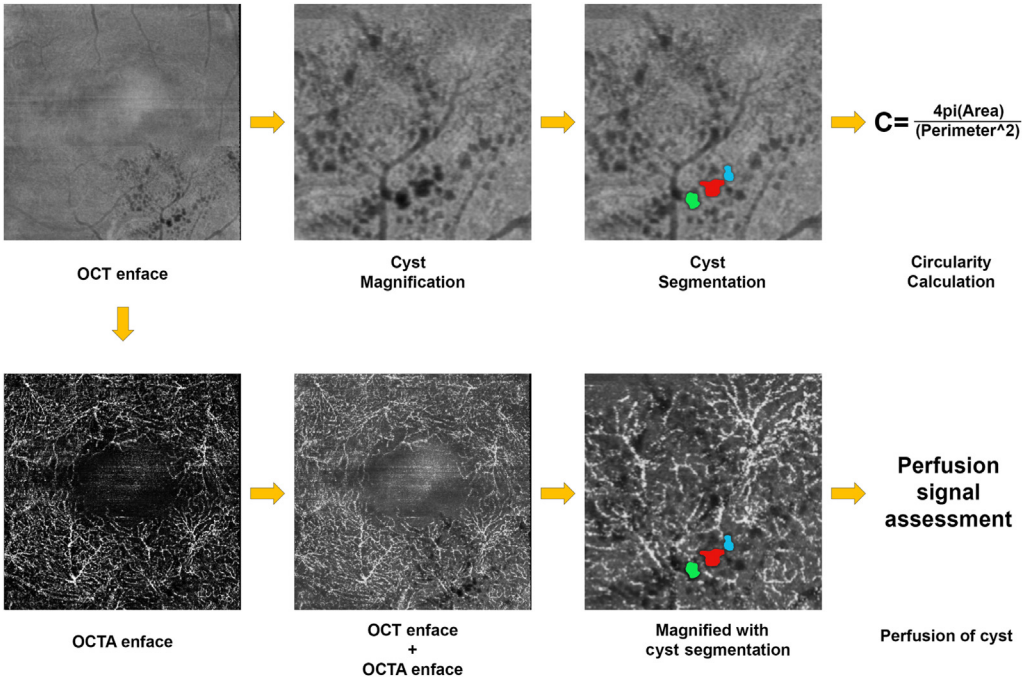

Figure 2. Schematic representation of cysts segmentation and perfusion signal assessment based on OCT enface segmentations. Starting from OCT enface, obtained placing segmentation slabs corresponding to the entire dimension of the cysts, we performed the automatic segmentation of each cyst, selecting only the black pixels (range, 0–20). Each cyst (manually colored in this figure) is separately considered for circularity calculation. The second step was overlapping the segmented cysts on enface OCTA reconstruction, obtained by using the same segmentation slabs of the cysts. In this way, it is possible to assess the perfusion status of each cyst, as described in the Methods section and visually represented in Figure 3. OCTA = OCT angiography.

used OCT images to assess the presence of subretinal fibrosis (defined as the presence of a subretinal or subretinal pigment epithelium hyperreflective lesion with multilaminar appearance) and outer retinal atrophy (defined as the loss of the ellipsoid and interdigitation zones associated with thinning of the outer nuclear layer, with or without decreased or absent retinal pigment epithelium and choroidal hypertransmission).[17]

Intraretinal Cyst OCTA Analyses

This part of the analysis was dedicated to assessing the relationship between each selected cyst and the intraretinal capillaries. Also, in this case, we used a combined approach based on enface OCTA scans and DART OCTA scans.

As, to our knowledge, no standardized method was available in the literature, we hypothesized that a cyst has a transudative/exudative origin if they are near intraretinal capillaries; we considered that "near" could be reasonably defined as located within double the segmented cyst's area. Otherwise, the cyst was considered a degenerative pseudocyst.

Starting from the segmented cyst on enface OCT, the first step was to enlarge the area of the cyst in ImageJ considering 1.5 and 2 factors (i.e., the two enlarged areas corresponded to [cyst area x 1.5] and [cyst area x 2], respectively). We then overlaid the enface OCT and OCTA reconstructions. For OCTA, we placed the layer segmentation lines corresponding to the upper and lower margins of the expanded cyst. Then, we selected the boundaries of the expanded cyst, and we subtracted all the background. If the vascular flow signal remained within the selected area, we classified the cyst as IRF with transudative/exudative origin. Otherwise, we classified the cyst as a degenerative pseudocyst. We used (area × 2) as the reference to classify the cysts. Moreover, we used (area × 1.5) to perform a stricter subanalysis regarding the perfusion status of each cyst.

The same process as described above was also performed for segmented cysts on structural OCT and DART images. In this case, we subtracted the background, considering only the doubled area of the cyst, and we checked if a DART signal was present or not within the selected area. This method is shown in Figure 3.

Evaluation of HF

We used structural OCT scans to evaluate the presence of hyperreflective foci (HF) in the context of the cysts. Hyperreflective foci are defined as small, round or dot-like hyperreflective lesions, >30 μm in diameter, without posterior shadowing.[18] We used the same segmentations described above (cyst area and cyst area × 2), and we analyzed the HF included in the (cyst area × 2). Because of the lack of standardized approaches, we arbitrarily considered HF number >5, calculated on all the OCT b-scans for each cyst, as a positive finding. We inverted the white-black color OCT b-scan to better highlight HF.

Statistical Analyses

All the analyses were performed by 2 expert graders (E.A. and M.B.P.) at least twice, to assess both reproducibility and repeatability for all the considered quantitative parameters.

Reproducibility and repeatability were assessed in accordance with the British Standards Institute and the International Organization for Standardization.[19] Furthermore, we calculated interclass correlation coefficients to assess the intergrader agreement using a 2-way random-effects model, provided in SPSS software (SPSS for Windows, Version 18.0, SPSS Inc).

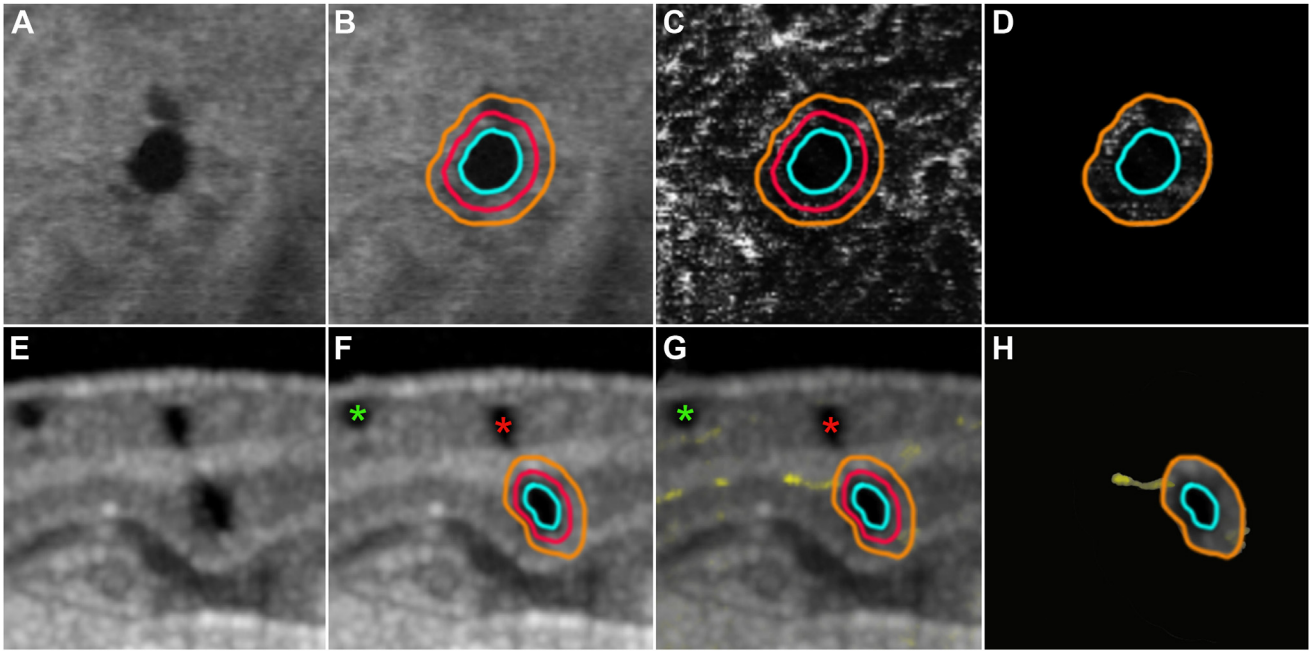

Figure 3. Schematic representation of perfusion signal assessment of intraretinal cysts based on OCT b-scan and enface segmentations. **A**, For OCT enface images, (**B**) the segmented cyst area (manually colored in blue) is enlarged by 1.5-fold (manually colored in red) and 2-fold (manually colored in orange). **C**, These segmentations are overlapped with enface OCTA reconstructions. **D**, Then, we selected only OCTA signals included in the red and orange areas to perform the assessment of the peri-cyst perfusion signal. Red demarcation is removed from the figure to better show the peri-cyst perfusion signal. **E**, The same steps are performed in a DART OCT B-scan, considering all the slabs showing the intraretinal cyst. **F**, Also in this case, the cyst area (manually colored in blue) is enlarged by 1.5-fold (manually colored in red) and twofold (manually colored in orange). **G**, Then, these areas were overlapped with the DART OCTA signal and only the OCTA signals included in the red and orange areas were selected to perform the assessment of peri-cyst perfusion signal. As shown in **H**, DART OCTA also can follow the course of intraretinal capillaries serving the cyst. The selected cyst is classified as an IRF cyst with perfusion. The other 2 cysts shown in the DART OCT B-scan are classified as an IRF cyst (green asterisk) and a degenerative cyst (red asterisk). The high-resolution DART OCT b-scan also highlights the round aspect of IRF cysts and the square aspect of degenerative pseudocysts. DART = dense automatic real-time; IRF = intraretinal fluid; OCTA = OCT angiography.

For the statistical analyses, age and sex were considered as fixed factors. We also included the following variables: total number of intravitreal anti-VEGF injections administered, duration of the disease (since the onset of neovascular AMD), presence of subretinal fibrosis, and outer retinal atrophy. We checked the distribution normality for each variable by frequency histograms and quantile-quantile plots. Continuous variables are reported as mean ± standard deviation, whereas categorical variables are reported as frequency and proportions. Continuous variables were analyzed by means of a 2-tailed t test. Mixed models were used to assess the relationships among the collected variables. P values ≤ 0.05 were considered statistically significant.

Results

Overall, we analyzed 387 cysts collected from 35 eyes of 35 patients with neovascular AMD (14 men; mean age 80 ± 5 years). The mean HEYEX quality score was 29 (range, 25−34). Mean BCVA was 0.50 ± 0.23 logarithm of the minimum angle of resolution (logMAR) (range, 0.1−1.0). The mean duration of neovascular AMD disease was 5 years (range, 3−9 years). Demographic and clinical data are reported in Table 1. The recruited patients had a minimum of 3 years of follow-up (maximum 9 years). Macular neovascularization were classified as type 1 (63%), type 2 (23%), or mixed type (14%), receiving a good number of intravitreal injections over the entire follow-up. Logarithm of the minimum angle of resolution BCVA significantly decreased as the duration of the disease increased ($P < 0.001$). Similarly, the incidence of fibrosis and atrophy significantly increased over time, starting from 25% and 37.5% at 3 years, respectively, and affected the entire cohort of eyes at ≥5 years' duration ($P < 0.001$).

We found IRF cysts in 35 of 35 eyes (100%), whereas we found degenerative pseudocysts in 21 of 35 eyes (60%). The results of the analyses are extensively reported in Table 2. Based on our analyses, we found 302 IRF cysts and 85 degenerative pseudocysts. All the cysts were localized in the innermost retinal layers, above the outer nuclear layer. Ten of 35 eyes showed no signs of fibrosis or outer retinal atrophy. All these eyes were characterized only by IRF cysts (mean number 16; range, 8−28). Six of 35 eyes were characterized only by outer retinal atrophy. Four eyes (67%) showed IRF cysts only (mean number 11; range, 8−18), whereas 2 eyes (33%) showed both IRF cysts and degenerative pseudocysts (mean number IRF cysts, 11; range, 10−12; mean number degenerative pseudocysts, 3; range, 3−3). The remaining 19 eyes showed both fibrosis and outer retinal atrophy. All these eyes were characterized both by IRF cysts and degenerative pseudocysts (mean number IRF cysts 7; range, 5−14; mean number degenerative pseudocysts 4; range, 2−8). With regard to the perfusion status of IRF cysts, we detected

Table 1. Demographic and Clinical Data

Characteristic	Value
Sex (M/F)	14/21
Age (yrs)	80 ± 5
Disease duration (yrs)	5 (range, 3–9)
No. of patients/follow-up	
1 yr	0
2 yr	0
3 yr	8
4 yr	7
5 yr	7
6 yr	5
7 yr	1
8 yr	3
9 yr	4
MNV type	
Type 1	22 (63%)
Type 2	8 (23%)
Mixed 1/2 type	5 (14%)
No. of intravitreal injections	
1 yr	5.6 (range, 3–7)
2 yr	4.7 (range, 3–6)
3 yr	3.9 (range, 2–5)
4 yr	3.4 (range, 2–5)
5 yr	2.7 (range, 1–4)
6 yr	2.3 (range, 1–3)
7 yr	2 (range, 1–3)
8 yr	1.7 (range, 1–3)
9 yr	2.3 (range, 2–3)
logMAR BCVA	
3 yr	0.33 (range, 0.1–0.6)
4 yr	0.41 (range, 0.2–0.6)
5 yr	0.44 (range, 0.3–0.6)
6 yr	0.50 (range, 0.4–0.7)
7 yr	0.90 (range, N/A)
8 yr	0.73 (range, 0.7–0.8)
9 yr	0.88 (range, 0.7–1.0)
Fibrosis	
3 yr	2/8 (25%)
4 yr	3/7 (43%)
5 yr	3/7 (43%)
6 yr	3/5 (60%)
7 yr	1/1 (100%)
8 yr	3/3 (100%)
9 yr	4/4 (100%)
Atrophy	
3 yr	3/8 (37.5%)
4 yr	4/7 (57%)
5 yr	5/7 (71%)
6 yr	5/5 (100%)
7 yr	1/1 (100%)
8 yr	3/3 (100%)
9 yr	4/4 (100%)

BCVA = best-corrected visual acuity; logMAR = logarithm of the minimum angle of resolution; MNV = macular neovascularization; N/A = not applicable.

perfusion signal within the (area × 1.5) ring in 255 of 302 cysts (84%) for enface OCTA and in 279 of 302 cysts (92%) for DART OCTA ($P < 0.001$). Considering the (area × 2) ring alone, we detected perfusion signal in 49 of 302 cysts (16%) for enface OCTA and in 23 out of 302 cysts (8%) for DART OCTA ($P < 0.001$). With respect to degenerative pseudocysts, the (area × 1.5) and (area × 2) rings were without perfusion signal in 100% of cases. An example of perfusion signal assessment in IRF cysts and degenerative pseudocysts is shown in Figure 4. We found statistically significant differences in cyst circularity between IRF cysts and degenerative pseudocysts: IRF cysts were significantly rounder (higher circularity) than degenerative pseudocysts, both on enface OCTA and DART OCTA images ($P < 0.001$). Comparing enface OCTA and DART OCTA findings in IRF cysts, circularity was very slightly but significantly higher in DART OCTA than enface OCTA (0.86, range, 0.81–0.91 vs. 0.85, range, 0.78–0.91; $P < 0.001$). Conversely, degenerative pseudocysts were slightly but significantly less round on DART OCTA than enface OCTA (0.68, range, 0.64–0.76 vs. 0.71, range, 0.66–0.79; $P = 0.003$).

Regarding HF surrounding the cysts, IRF cysts were surrounded by HF in 31 of 35 (89%) eyes, compared with degenerative pseudocysts, which showed HF in only 6 of 21 eyes (29%) ($P < 0.001$). Of 302 IRF cysts, we found HF in 260 cysts (86%), whereas we detected HF in 18 of 85 degenerative pseudocysts (21%) ($P < 0.001$). An example case of HF assessment is shown in Figure 5.

More IRF cysts correlated with lower incidence of fibrosis and atrophy (Kendall's τ coefficient −0.549 and −0.477, respectively; $P < 0.001$). Conversely, the higher the number of degenerative pseudocysts, the higher the incidence of fibrosis and atrophy (Kendall's τ coefficient 0.770 and 0.619, respectively; $P < 0.001$). As a direct consequence, BCVA (expressed in LogMAR) showed an inverse significant correlation with the number of IRF cysts (Kendall's τ coefficient −0.516; $P < 0.001$) and a direct significant correlation with degenerative pseudocysts (Kendall's τ coefficient 0.699; $P < 0.001$). Similar results were found considering disease duration (Kendall's τ coefficient −0.759 for IRF cysts and 0.607 for degenerative pseudocysts; $P < 0.001$). Interestingly, we found a direct, significant correlation between the number of degenerative pseudocysts and the number of injections administered from year 5 to year 9 (overall Kendall's τ coefficient 0.550; $P < 0.001$). Moreover, we found an inverse significant correlation between the number of IRF cysts and the number of injections administered from year 4 to year 9 (overall Kendall's τ coefficient −0.520; $P < 0.001$).

Reproducibility and repeatability values for all the measures are reported in Table 3.

Discussion

This study aimed to propose an automatic way to categorize intraretinal cysts based on quantitative characteristics: a newly introduced OCTA-based perfusion assessment in the vicinity of the cysts, paired with the cyst circularity calculation. We found statistically significant differences between IRF cysts and degenerative pseudocysts, considering both approaches. The complete lack of perfusion signal of degenerative pseudocysts provides further support to the interpretation of these OCT findings as empty spaces secondary to the advanced deterioration of retinal anatomy.[10–12] Similarly, the very frequent presence of perfusion signal in the vicinity of IRF cysts supports the theory of inner blood–retinal barrier and Müller cell impairment as the main source of IRF.[8,9] Indeed, it stands to

Table 2. IRF Cysts versus Degenerative Pseudocysts

Parameter	IRF Cysts	Degenerative Pseudocysts	*P*
No. of eyes	35/35 (100%)	21/35 (60%)	
No. of cysts	302	85	
No. of cysts with perfusion only within (area × 1.5) enface OCTA	255/302 (84%)	0	
No. of cysts with perfusion only within (area × 2) enface OCTA	49/302 (16%)	0	
N. of cysts with perfusion only within (area × 1.5) DART OCTA	279/302 (92%)	0	<0.05
No. of cysts with perfusion only within (area × 2) DART OCTA	23/364 (8%)	0	
Circularity cysts enface OCTA	0.85 (range, 0.78–0.91)	0.71 (range, 0.66–0.79)	
Circularity cysts DART OCTA	0.86 (range, 0.81–0.91)	0.68 (range, 0.64–0.76)	
HF in peri-cysts region (No. of eyes)	31/35 (89%)	6/21 (29%)	

DART = dense automatic real-time; HF = hyperreflective foci; IRF = intraretinal fluid; OCTA = OCT angiography.

reason that blood flow should be present nearby the IRF cysts, although it may be inadequately regulated due to the known disturbance in IRF homeostasis in AMD.

In this study, we tested both enface OCTA and DART OCTA to assess whether both approaches yield similar results. Looking at perfusion signal sampling, both techniques detected blood flow signal in the vicinity of IRF cysts, although DART OCTA did so significantly more frequently and, in the opinion of the authors, with a higher level of detail than enface OCTA. This may be due to the higher OCTA signal quality characterizing DART (due to substantially increased image averaging) compared with standard OCTA. Conversely, we have to point out the restricted field of view of DART OCTA, being limited to a maximum of 10° × 0.5° retinal eccentricity, as compared with standard OCTA, which allows a much wider assessment (in this

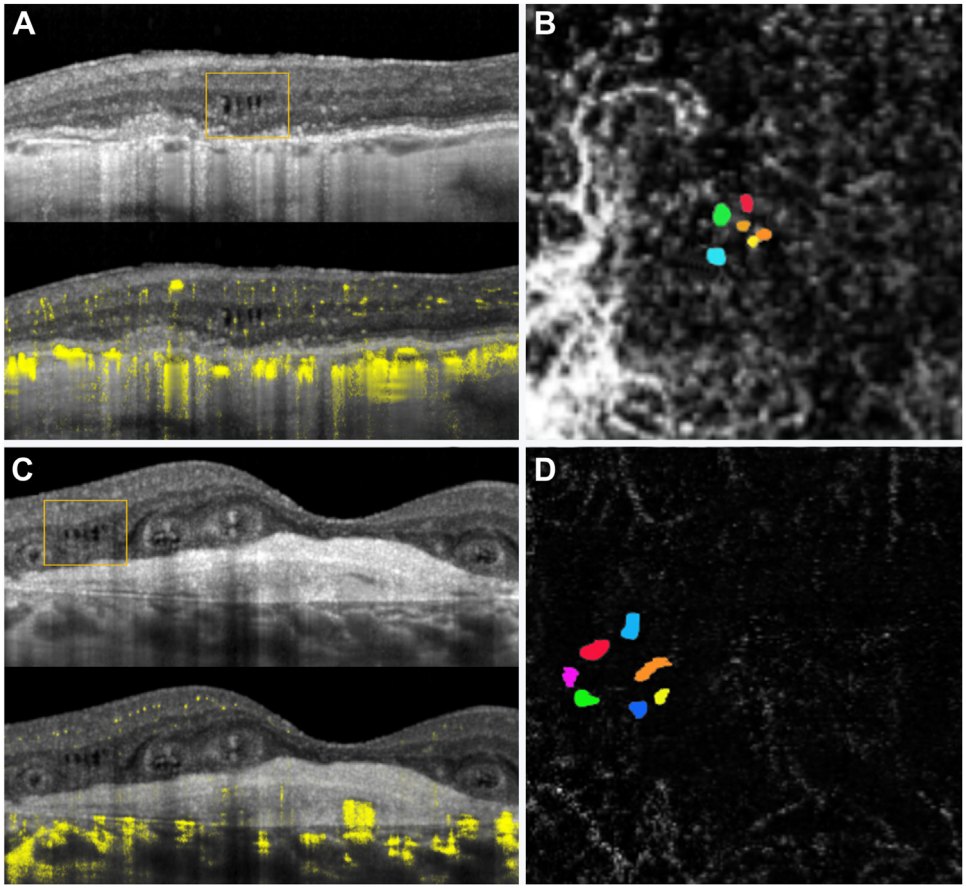

Figure 4. Multimodal imaging of IRF cysts and degenerative pseudocysts. The qualitative appearance of (**A**) IRF cysts and (**C**) degenerative pseudocysts (highlighted by orange squares) looks similar in terms of intraretinal localization. However, IRF cysts are characterized by a higher number of HF surrounding the cysts and evident peri-cyst perfusion signal, as highlighted by (**A**, **C**) DART OCTA and (**B**, **D**) enface OCTA. Moreover, IRF cysts and degenerative pseudocysts differ in terms of roundness, with degenerative pseudocysts looking more like squares than circles (also highlighted by the significantly different circularity values). DART = dense automatic real-time; IRF = intraretinal fluid; OCTA = OCT angiography.

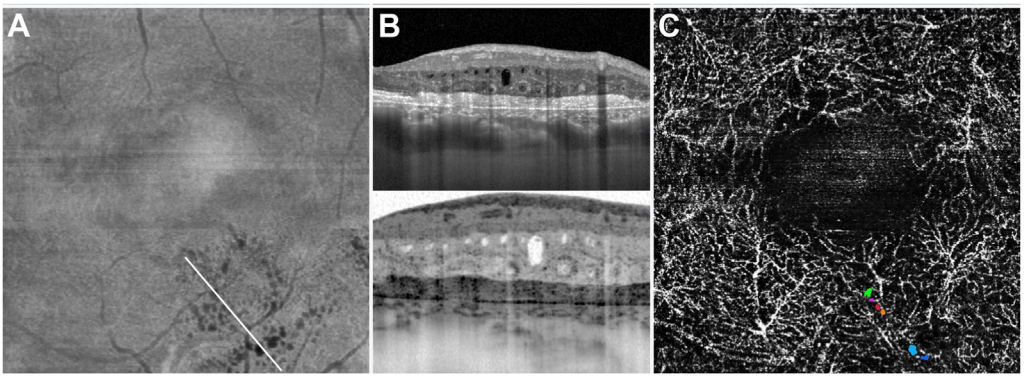

Figure 5. HF in IRF cysts. **A**, Enface OCT shows the slab (white line) corresponding to the (**B**) OCT b-scan. As highlighted by the inverted black-white colors, these intraretinal cysts, classified as IRF cysts, supported by the evidence of peri-cysts perfusion signal (**C**), are surrounded by a high number of HF. On enface OCTA, the selected IRF cysts are manually colored. HF = hyperreflective foci; IRF = intraretinal fluid; OCTA = OCT angiography.

study, 15° × 15° retinal eccentricity). For this reason, although DART OCTA may be recommended to collect many more details, enface OCTA should be preferred for a more comprehensive assessment of the macular area. Considering circularity calculation, DART OCTA provided significantly higher values for IRF cysts compared with enface OCTA, as well as significantly lower values for degenerative pseudocysts, although the value differences did seem small. These differences might be related to the higher digital resolution (sampling) of DART b-scan OCT, compared with enface OCT, and to the different approaches of circularity calculation. Dense ART scans have resolution of ∼5.9 μm/pixel both along and between b-scans, whereas regular OCTA used in this study had 5.9 μm/pixel along b-scans but ∼11 μm between b-scans. Cyst segmentation was performed on the enface OCT segmentation considered in its entirety; for DART images, this was performed b-scan by b-scan, which could provide a more precise calculation of the circularity. The advantage is a more precise segmentation of the cysts, although the procedure requires more images, which is potentially time consuming. In addition, previous studies reported that degenerative pseudocysts are characterized by a square-like aspect, compared with the roundness profile of IRF cysts.[10–12] We might advance the hypothesis that the squareness or roundness of intraretinal cysts is more pronounced in the *x-y* axes (OCT b-scan) than in *z* axis (enface OCT), based on our findings. That said, the chosen segmentation approach, based on the automatic selection of black pixels instead of manual segmentation, allowed us to avoid manual input, and accordingly, our calculation is highly reproducible and repeatable, as reported in Table 3, as well as potentially adoptable for AI-based automatic methodologies.

The detection and categorization of macular fluids is a major topic of current research, especially considering the employment of AI-based approaches.[13] These technologies facilitate the monitoring of the disease and the individuation of clinically relevant biomarkers.[13,20] The sensitivity of AI algorithms for detecting retinal fluids is very high[13,16,20]; however, to our knowledge, the current literature is focused in discriminating IRF from other types of fluid with a paucity of studies on AI-based discrimination of different types of intraretinal cysts. Given the different clinical implications of IRF cysts and degenerative pseudocysts in terms of disease severity and progression patterns,[10–12] it is fundamental for AI tools to categorize them. The major challenge of AI training is the individuation of reliable metrics to be introduced in the calculation. As shown in Figure 4, the qualitative features of IRF cysts and degenerative pseudocysts look similar, complicating the proper categorization by AI tools.

As an additional finding, many more HF were observed surrounding IRF cysts compared with degenerative pseudocysts. Hyperreflective foci are commonly interpreted as activated monocytes–microglial cells and a sign of disease activity.[21] Therefore, detecting more HF in IRF cysts than in inactive degenerative pseudocysts is perhaps not surprising. The presence of HF in the context of degenerative pseudocysts might be interpreted as a sign of still-present disease activity or as remnants of other retinal cytotypes. However, this hypothesis would benefit from future histologic validations.

The separate assessment of IRF and degenerative pseudocysts may have clinically significant implications: we

Table 3. Reproducibility and Repeatability of the Measures

Parameter	Reproducibility	Repeatability
Circularity calculation enface OCTA	0.98 (range, 0.95–0.99)	0.98 (range, 0.96–0.99)
Circularity calculation DART OCTA	0.98 (range, 0.94–0.99)	0.98 (range, 0.94–0.99)
Cysts perfusion calculation	0.95 (range, 0.89–0.98)	0.96 (range, 0.89–0.98)
HF assessment	0.96 (range, 0.90–0.98)	0.97 (range, 0.90–0.98)

DART = dense automatic real-time; HF = hyperreflective foci; OCTA = OCT angiography.

found associations with the duration of the disease, number of intravitreal injections, fibrotic–atrophic evolution, and visual function. Interestingly, we found a direct relationship between the number of degenerative pseudocysts and the number of injections administered from year 5 to year 9, indicating that more active disease—requiring more injections—is associated with higher risk of degenerative phenomena in the long term. Conversely, we found an inverse relationship between the number of IRF cysts and the number of injections administered from year 4 to year 9, further supporting the already known statement that proactive strategies with a high number of intravitreal injections should be preferred to guarantee optimal management of the disease and lower retinal fluid fluctuations in the long term.[22] Moreover, we found an inverse significant correlation between logMAR BCVA and the number of IRF cysts, as well as a direct significant correlation with degenerative pseudocysts. This finding might be related to the longer disease duration characterizing eyes with degenerative pseudocysts, as well as more aggressive lesions, as supported by the higher number of injections administered, leading to worse deterioration of visual function.

We are aware that our study has several limitations and that it should be considered as a preliminary study, outlining a possible quantitative approach to be tested with AI-based algorithms. A major limitation is the relatively low number of eyes included. The methodological strategies were planned to maximize the robustness of the analyses, minimizing the impact of potential biases and confounding factors. However, the analyses performed here were time consuming, which makes them poorly applicable in clinical practice. The criteria adopted to categorize IRF cysts from degenerative pseudocysts have been arbitrarily chosen. Despite the presence of OCT signs of terminal degeneration, we cannot exclude at all that some cysts classified as degenerative pseudocysts might be persistent IRF cysts. However, the findings provided by the entire multimodal imaging analysis support the hypothesis that IRF cysts and degenerative pseudocysts are characterized by significantly different OCT and OCTA characteristics, which can be used to categorize these lesions. Moreover, quantitative OCTA analyses depend on high-quality images although they can be affected by several artifacts, which are more common in the presence of retinal angiomatous proliferation or polypoidal choroidal vasculopathy.[23–25] The inclusion of eyes with 3 to 9 years' duration meant that retinal structures were altered in most of the cases. This fact, together with the inclusion of cysts with a diameter of >50 μm, determined the fact that more retinal layers were involved by the cysts. For these reasons, we could not provide data regarding the precise localization of IRF cysts and degenerative pseudocysts. We also applied a simple binary classification of atrophy and fibrosis that was adopted in preference to an accurate quantification. Some selection parameters, such as the assessment of the relationship of IRF cysts and degenerative pseudocysts with intraretinal capillaries, or the threshold of ≥5 HF, were chosen based on a scientific guess, in the absence of standardized guidelines; this would thus require further validation. Moreover, the eyes were treated in a real-life setting, accordingly to the ophthalmologists' discretion. For this reason, it was not possible to perform analyses focused on the effect of treatment strategies in the quantitative analyses performed in this study. Further investigations are warranted to test the relationship between intravitreal treatments and the quantitative characteristics of IRF cysts and degenerative pseudocysts. Lastly, our study was designed as a cross-sectional investigation. Future prospective longitudinal studies are warranted to support the clinical relevance of the present findings.

In conclusion, the present study proposed a quantitative approach to categorize IRF cysts and degenerative pseudocysts. This approach holds promise as a clinical assessment in the neovascular AMD setting. We also tested the different contribution of DART OCTA and enface OCTA approaches. Overall, we are of the opinion that DART OCTA provides more details on blood flow than enface OCTA, although it is significantly limited by the small field of view. Future studies should be focused on the implementation of this quantitative strategy in the development of AI-based tools, to improve the amount of information provided by this technology and to optimize the diagnostic workup of patients with neovascular AMD.

Acknowledgments

The authors mourn the recent loss of Professor Ramin Tadayoni, MD, PhD (Ophthalmology Department, AP-HP, Hôpital Lariboisière, Université de Paris, Paris, France), who participated in developing this research and was included as last author in preliminary versions of the manuscript. The contribution provided by Professor Tadayoni was fundamental for the conduction of this study. The authors will be forever grateful to Professor Tadayoni for his energy, enthusiasm, and desire to transmit and improve knowledge that has characterized him during this study and in all aspects of his outstanding career.

The authors also acknowledge Michel Teussink, PhD (Michel.Teussink@HeidelbergEngineering.com) (Heidelberg Engineering GmbH, Heidelberg, Germany) for the unrestricted contribution to data analysis and interpretation.

Footnotes and Disclosures

Originally received: March 25, 2024.
Final revision: May 22, 2024.
Accepted: May 24, 2024.
Available online: June 6, 2024. Manuscript no. ORET-D-24-00286R2.

[1] Department of Ophthalmology, IRCCS San Raffaele Scientific Institute, Milan, Italy.

[2] Eye Repair Unit, Division of Neuroscience, IRCCS San Raffaele Scientific Institute, Milan, Italy.

Disclosure(s):

All authors have completed and submitted the ICMJE disclosures form.

The authors have no proprietary or commercial interest in any materials discussed in this article.

HUMAN SUBJECTS: Human subjects were included in this study. The study was approved by the Ethical Committee of the IRCCS San Raffaele Scientific Institute, Milan (referral code MIRD2020) and conducted in accordance with the Declaration of Helsinki. A signed informed consent was obtained from all patients before inclusion in the study.

No animal subjects were used in this study.

Author Contributions:

Conception and design: Arrigo, Aragona

Data collection: Arrigo, Aragona, Parodi, Bandello

Analysis and interpretation: Arrigo, Aragona, Parodi, Bandello

Obtained funding: N/A

Overall responsibility: Arrigo, Aragona, Parodi, Bandello

Abbreviations and Acronyms:
AI = artificial intelligence; **AMD** = age-related macular degeneration; **ART** = automatic real-time; **BCVA** = best-corrected visual acuity; **DART** = dense ART; **HF** = hyperreflective foci; **IRF** = intraretinal fluid; **logMAR** = logarithm of the minimum angle of resolution; **MNV** = macular neovascularization; **OCTA** = OCT angiography.

Keywords:
Age-related macular degeneration, Degenerative pseudocysts, Intraretinal cysts, OCT, OCTA.

Correspondence:
Alessandro Arrigo, MD, PhD, via Olgettina 60, Milan, 20132, Italy. E-mail: alessandro.arrigo@hotmail.com.

References

1. Jung JJ, Chen CY, Mrejen S, et al. The incidence of neovascular subtypes in newly diagnosed neovascular age-related macular degeneration. *Am J Ophthalmol*. 2014;158:769–779.e2.
2. Schmidt-Erfurth U, Chong V, Loewenstein A, et al. Guidelines for the management of neovascular age-related macular degeneration by the European Society of Retina Specialists (EURETINA). *Br J Ophthalmol*. 2014;98:1144–1167.
3. Farecki ML, Gutfleisch M, Faatz H, et al. Characteristics of type 1 and 2 MNV in exudative AMD in OCT-angiography. *Graefes Arch Clin Exp Ophthalmol*. 2017;255:913–921.
4. Saenz-de-Viteri M, Recalde S, Fernandez-Robredo P, et al. Role of intraretinal and subretinal fluid on clinical and anatomical outcomes in patients with neovascular age-related macular degeneration treated with bimonthly, treat-and-extend and as-needed ranibizumab in the In-Eye study. *Acta Ophthalmol*. 2021;99:861–870.
5. Sadda S, Holekamp NM, Sarraf D, et al. Relationship between retinal fluid characteristics and vision in neovascular age-related macular degeneration: HARBOR post hoc analysis. *Graefes Arch Clin Exp Ophthalmol*. 2022;260:3781–3789.
6. Riedl S, Vogl WD, Waldstein SM, et al. Impact of intra- and subretinal fluid on vision based on volume quantification in the HARBOR trial. *Ophthalmol Retina*. 2022;6:291–297.
7. Lally DR, Hill L, Amador-Patarroyo MJ. Subretinal fluid resolution and visual acuity in patients with neovascular age-related macular degeneration: a HARBOR post hoc analysis. *Ophthalmol Retina*. 2022;6:1054–1060.
8. Sharma A, Kumar N, Parachuri N, et al. Understanding the mechanisms of fluid development in age-related macular degeneration. *Ophthalmol Retina*. 2021;5:105–107.
9. Hilely A, Au A, Freund KB, et al. Non-neovascular age-related macular degeneration with subretinal fluid. *Br J Ophthalmol*. 2021;105:1415–1420.
10. Cohen SY, Dubois L, Nghiem-Buffet S, et al. Retinal pseudocysts in age-related geographic atrophy. *Am J Ophthalmol*. 2010;150:211–217.e1.
11. Querques G, Coscas F, Forte R, et al. Cystoid macular degeneration in exudative age-related macular degeneration. *Am J Ophthalmol*. 2011;152:100–107.e2.
12. Monje-Fernández L, Gallego-Pinazo R, Cordero-Coma M, et al. Evaluation of non-exudative tomographic signs in cases of exudative age-related macular degeneration. *Arch Soc Esp Oftalmol (Engl Ed)*. 2023;98:276–280.
13. Schmidt-Erfurth U, Reiter GS, Riedl S, et al. AI-based monitoring of retinal fluid in disease activity and under therapy. *Prog Retin Eye Res*. 2022;86:100972.
14. Schmidt-Erfurth U, Mulyukov Z, Gerendas BS, et al. Therapeutic response in the HAWK and HARRIER trials using deep learning in retinal fluid volume and compartment analysis. *Eye (Lond)*. 2023;37:1160–1169.
15. Pawloff M, Gerendas BS, Deak G, et al. Performance of retinal fluid monitoring in OCT imaging by automated deep learning versus human expert grading in neovascular AMD. *Eye (Lond)*. 2023;37:3793–3800.
16. Schindelin J, Arganda-Carreras I, Frise E, et al. Fiji: an open-source platform for biological-image analysis. *Nat Methods*. 2012;9:676–682.
17. Spaide RF, Jaffe GJ, Sarraf D, et al. Consensus nomenclature for reporting neovascular age-related macular degeneration data: Consensus on Neovascular Age-Related Macular Degeneration Nomenclature Study Group. *Ophthalmology*. 2020;127:616–636.
18. Coscas G, De Benedetto U, Coscas F, et al. Hyperreflective dots: a new spectral-domain optical coherence tomography entity for follow-up and prognosis in exudative age-related macular degeneration. *Ophthalmologica*. 2013;229:32–37.
19. British Standards Institution. Precision of Test Methods I: Guide for the Determination and Reproducibility for a Standard Test Method *(BS 5497, Part I)*. London: BSI; 1979.
20. Keenan TDL, Clemons TE, Domalpally A, et al. Retinal specialist versus artificial intelligence detection of retinal fluid from OCT: Age-Related Eye Disease Study 2: 10-year follow-on study. *Ophthalmology*. 2021;128:100–109.
21. Fragiotta S, Abdolrahimzadeh S, Dolz-Marco R, et al. Significance of hyperreflective foci as an optical coherence tomography biomarker in retinal diseases: characterization and clinical implications. *J Ophthalmol*. 2021;2021:6096017.
22. Chakravarthy U, Havilio M, Syntosi A, et al. Impact of macular fluid volume fluctuations on visual acuity during anti-VEGF therapy in eyes with nAMD. *Eye (Lond)*. 2021;35:2983–2990.
23. Spaide RF, Fujimoto JG, Waheed NK. Image artifacts in optical coherence tomography angiography. *Retina*. 2015;35:2163–2180.
24. Spaide RF, Fujimoto JG, Waheed NK, et al. Optical coherence tomography angiography. *Prog Retin Eye Res*. 2018;64:1–55.
25. Arrigo A, Aragona E, Battaglia Parodi M, Bandello F. Quantitative approaches in multimodal fundus imaging: State of the art and future perspectives. *Prog Retin Eye Res*. 2023;92:101111.